ITER Relevant Simulations of Lower Hybrid and Ion Cyclotron Waves with Self-Consistent Non-Maxwellian Species

J. C. Wright 1), E. F. Jaeger 2), E. J. Valeo 3), D. B. Batchelor 2), L. A. Berry 2), P. T. Bonoli 1), C. K. Phillips 3), R. Bilato 4), M. Brambilla 4), E. F. D'Azevedo 2), R. W. Harvey 5), D. A. D'Ippolito 6), J. R. Myra 6), D. N. Smithe 7), and M. Choi 8)

1) PSFC, MIT, Cambridge, MA 02139, USA
2) ORNL, Oak Ridge, TN 37831, USA
3) PPPL, Princeton University, Princeton, NJ 08540, USA
4) Max-Planck-Institut für Plasmaphysik - Garching bei München, Germany
5) CompX, Del Mar, CA 92014, USA
6) Lodestar Research Corporation, Boulder, CO 80301 USA
7) Tech-X Corporation, 5621 Arapahoe Avenue, Boulder, Colorado 80303 USA
8) General Atomics, San Diego, CA 92186 USA

e-mail contact of main author: jwright@psfc.mit.edu

Abstract. The next step toward fusion as a practical energy source is the design and construction of ITER. ITER relies in part on ion-cyclotron radio frequency (ICRF) power to heat the deuterium-tritium plasma to fusion temperatures as well as to provide a portion of the current during flat-top operations. Lower hybrid (LH) RF power is under consideration as an upgrade to the baseline heating and current drive system in order to provide control over the current profile and additional current during start up. We have applied a suite of mature radio frequency (rf) full wave codes using self-consistent particle distributions from a Fokker-Planck code to ITER ICRF scenarios and ITER relevant LH experiments on Alcator C-Mod. We will present three dimensional full-wave simulations showing that the ICRF waves propagate radially inward in ITER with strong central focusing and little toroidal spreading. Fokker-Planck coupled rf simulations show that because of the high plasma density, energetic ion tail formation in ITER is typically weak, with the exception of the minority deuterium heating scheme where strong tails can develop on the minority ion distribution. Absorption by the fast alpha particles can approach five to ten percent of the injected power. Massively parallel full wave simulations in the lower hybrid range of frequencies using 2000 poloidal modes and 1000 radial elements have shown that proper reconstruction of wave fronts in the full wave treatment at caustics and cut-offs, where WKB methods fail, can lead to significant spectral broadening. We demonstrate that this linear mechanism is sufficient to bridge the spectral gap (the difference between the high injected phase velocities and the slower phase velocity at which damping on electrons occurs) and explains the efficient damping of lower hybrid waves. This is seen to affect the amount of broadening in the phase velocity and the current drive location.

1. Introduction

High-power radio frequency waves in the ion-cyclotron range of frequencies (ICRF) have the potential to heat and control the ITER [1] plasma through localized energy deposition, driven current, and driven plasma flows. ITER relies in part on ion-cyclotron radio frequency power to heat the deuterium and tritium fuel to fusion temperatures. Heating scenarios being considered include majority T at the second harmonic frequency, minority He^3 at the fundamental frequency, and for early low field operation, minority D at the fundamental frequency [2]. Depending on the specific case, wave-plasma interactions can include mode conversion, parasitic absorption on fast ion components, and energetic ion tail formation. All of these processes will require accurate modelling and complete theoretical understanding if we are to realize the potential of ICRF wave power to heat and control the ITER plasma. Lower hybrid waves (LH) are under consideration for off axis current drive on ITER [3]. To reach the target current profiles having an internal inductance of $l_i(3)$~[0.6-0.8], some off-axis current profile control may be necessary and at reactor grade temperatures, LH waves will

experience strong single pass absorption at large minor radius (r/a>0.7). Advanced LH simulation codes treat wave propagation in the geometrical optics limit using ray tracing, which is known to neglect important effects on the wave spectrum due to focusing, diffraction, and proper wave front reconstruction at cut-offs [4]. For some parameters, full wave predictions of power deposition differ significantly from those of ray tracing [5]. Accurate modeling of all relevant physical processes will be needed to reliably control the current profile in modern and reactor relevant devices.

Previous calculations in the SciDAC Center for Simulation of Wave-Plasma Interactions [6] have laid the foundation for this understanding by developing and applying advanced wave solvers [7-9] and demonstrating the feasibility of coupling to Fokker-Planck solvers [10]. In this paper, these calculations are extended to the burning plasma regime of ITER where the combination of physical size and high plasma density require an order of magnitude higher resolution than previous calculations. To meet this challenge, the AORSA global-wave solver [7] has been tuned for use on multi-core processing architectures [11], with the result of this approach that execution on the dual-core Cray XT-4 at Oak Ridge National Laboratory, named Jaguar, has demonstrated excellent scaling up to tens of thousands of processors as shown achieving 87.5 trillion calculations per second (87.5 teraflops) which is about 73% of the system's theoretical peak. We have also developed a parallel version of the TORIC full-wave electromagnetic field solver valid in the LH range of frequencies with a non-Maxwellian electron dielectric [5,12]. The diffraction observed in the full wave code is sufficiently strong to downshift the wave phase speed, causing the LH waves to damp at r/a~0.75 in a 4 keV plasma. We note that the full-wave treatment described in this paper should be more accurate than methods that employ paraxial beam tracing algorithms [13].

The rest of this paper is organized as follows: after summarizing the full wave equations for ICRF in Section 2 we analyze two ITER scenarios in which three dimensional and non-Maxwellian effects play an important role in the following two sections. In Section 5 the lower hybrid problem is introduced and the need to include full wave effects is demonstrated in subsequent sections.

2. Wave-plasma Interactions in the Ion Cyclotron Range of Frequencies

For rapidly oscillating, time-harmonic wave fields propagating in a plasma, Maxwell's equations reduce to a generalization of the Helmholtz wave equation,

$$\begin{aligned}
\boldsymbol{\nabla}\times\boldsymbol{\nabla}\times\mathbf{E} &= \frac{\omega^2}{c^2}\left\{\mathbf{E}+\frac{4\pi i}{\omega}\left(\mathbf{J}^{\mathrm{P}}+\mathbf{J}^{\mathrm{A}}\right)\right\} \\
\mathbf{E}(\mathbf{x}) &= \sum_{lmn}\mathbf{E}_{lmn}\exp\left(ilk_R^0R+imk_Z^0Z+in\phi\right) \\
k_{\|}^{lmn}\mathbf{E}_{lmn} &= \mathbf{B}\cdot\boldsymbol{\nabla}\mathbf{E}/B=(lB_R+mB_Z+nB_\phi)/B\mathbf{E}_{lmn} \\
\mathbf{J}^{\mathrm{P}}(\mathbf{x}) &= \sum_{lmn}\sigma_c\left(k_{\|}^{lmn},\mathbf{x}\right)\cdot\mathbf{E}_{lmn}
\end{aligned} \quad , \qquad (1)$$

where $\mathbf{J}^{\mathbf{A}}$ is the externally driven antenna current at frequency ω, and $\mathbf{J}^{\mathbf{P}}$ is the fluctuating plasma current. The plasma current can be written as a non-local, integral operator on the wave electric field **E**, where σ_c is the plasma conductivity tensor [14]. This integro-differential equation is solved for arbitrary non-Maxwellian distributions by AORSA [7], a two

dimensional spectral wave solver, using a plasma conductivity valid to all orders in the ion Larmor radius and retaining all cyclotron harmonics. AORSA employs a fully spectral basis set in toroidal-polar coordinates, R, Z and φ.

Multiple non-thermal particle populations due to wave heating, neutral beam injection, and fusion reactions may exist simultaneously, can absorb power at high harmonics of the ion cyclotron frequency, and can have a significant effect on the wave propagation and absorption. To self-consistently simulate the rf propagation and absorption and the plasma particle distribution response we couple the wave equation and a Fokker-Planck equation for the particle response with a quasilinear rf operator,

$$\frac{\partial}{\partial t}(\lambda f_0) = \nabla_{u_0} \cdot \Gamma_{u_0} + \langle\langle R \rangle\rangle + \langle\langle S \rangle\rangle \qquad (2)$$

where f_0 is the bounce-averaged ion distribution function evaluated at the outer equatorial plane, λ is the bounce period normalized to the free streaming parallel passing period, and $\langle\langle S \rangle\rangle$ is a bounce-averaged particle source/sink operator. The radial diffusion operator $\langle\langle R \rangle\rangle$ is assumed to be zero for calculations in this paper. The divergence term in Eq. (2) contains two parts: the collision operator $C(f_0)$ that describes slowing down due to collisions and the quasi-linear operator $Q(f_0,\mathbf{E})$ that describes diffusion in velocity space due to the wave electric field [15]. Equation (2) is solved by CQL3D [16] a three dimensional(3D), bounce-averaged Fokker-Planck solver that uses the zero orbit width approximation for particle orbits. The non-linear system comprised of Eq.(1) and (2) is solved by iterating between the AORSA and CQL3D codes to reach the steady state solution.

3. Ion Cyclotron Heating at $2\Omega_T$ for Scenario#2 in ITER

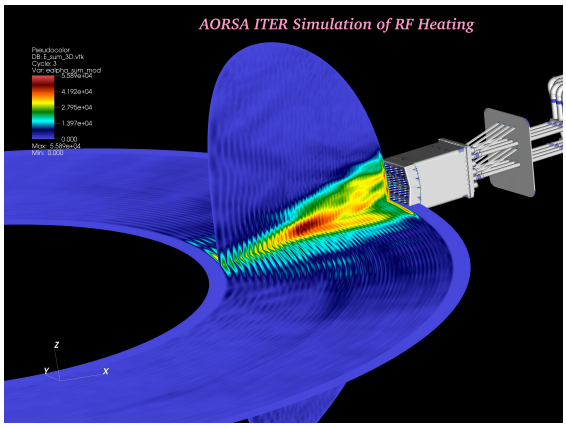

FIG. 1. 3D simulation of ITER Scenario#2, 2nd harmonic Tritium heating. Plasma parameters are: major radius R = 6.2 m, toroidal magnetic field B = 5.3 T, central electron density $n_e(0)$=1.02 x 1020 m^{-3}, central electron temperature $T_e(0)$ = 24.8 keV, and central ion temperature $T_i(0)$ = 21.2 keV.

We first apply this model to Scenario#2 for ITER [17]. Important parameters for the ICRF heating system are source frequency $\omega/2\pi$ = 53 MHz, antenna height 1.76 m, antenna position R_{ANT} = 8.165 m, and ICRF power P_{rf} = 20 MW. The plasma composition is 31.66 % deuterium (D), 50% tritium (T), 2% beryllium (Be), 4.41% helium ash (He^4), and 0.761% fast fusion alpha particles. Figure 1 shows a 3D visualization from AORSA for the Elmy H-mode plasma in ITER Scenario#2 constructed from a series of two dimensional solutions with different toroidal mode numbers. The 2nd harmonic tritium resonance is located at R=6.514 cm for the parameters given in the figure. The fast magnetosonic wave is used to penetrate to the center of the dense core plasma where it is absorbed at the second harmonic cyclotron resonance of tritium. Wave power is also absorbed by electrons directly through electron Landau damping and magnetic pumping, and indirectly through collisions with the ions. These are the primary absorption mechanisms in

the absence of additional minority ions such as He^3. The high plasma beta in ITER results in strong absorption on electrons and in this case the power partition is roughly split between electrons (48.7%) and tritium (48.7%).

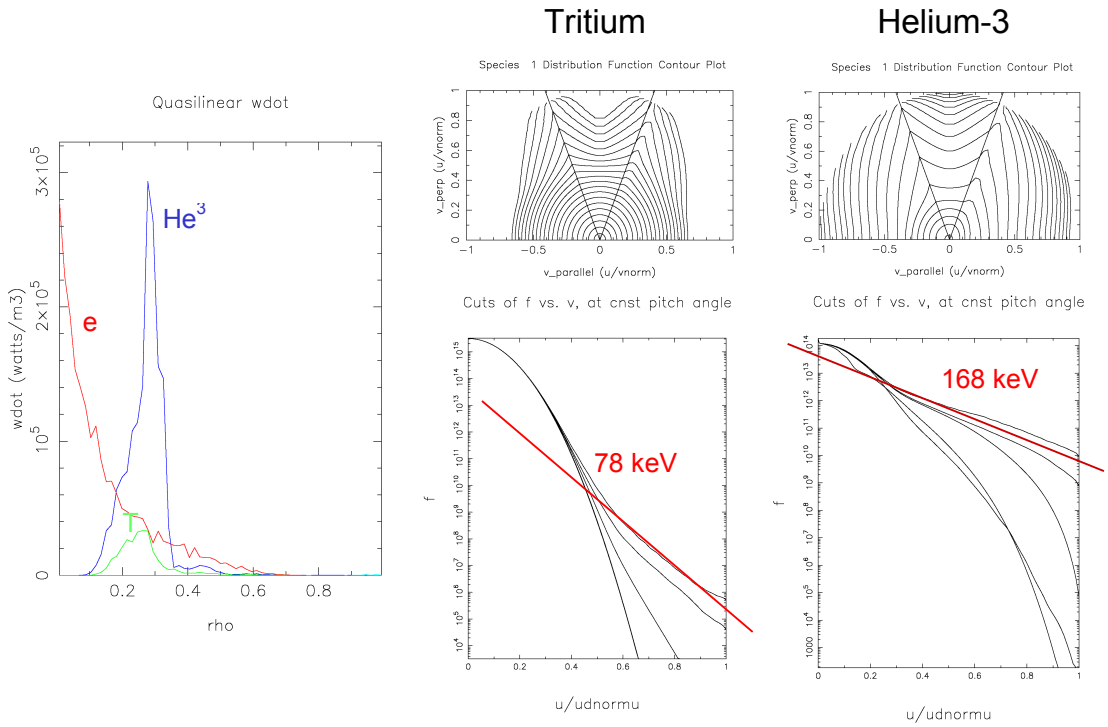

FIG. 2. Self-consistent heating profiles and minority ion distribution function for a minority He^3 heating scheme in ITER (r/a = 0.270 and n = -27).

The visualization in FIG. 1 shows the 3D wave fields from AORSA with a close-up of the antenna structure (~2m high). It shows the highly focused wave fronts in both poloidal and equatorial planes. A correlation between the high rf field regions at the plasma edge and the antenna can clearly be seen. An ongoing task is to minimize these “hot spots” and to provide adequate protection and cooling for the antenna. Three dimensional visualizations such as these are becoming increasingly important for understanding and using the results of large simulations like AORSA such as of the antenna-edge interactions in ITER.

4. ICRF Interactions with Non-Maxwellian Distributions

We turn now to the case of minority heating of He^3 in which taking non-thermal distributions into account is important. Whereas in the case considered in Section 3, the plasma response could be considered Maxwellian because the wave interactions were with the bulk electrons and ions (or in the case of alpha particles, the small concentrations used could be modelled with high temperature effective Maxwellians), minority heating creates large non-thermal tails. The fundamental resonance for He^3 occurs at the same location as the second harmonic resonance for tritium, and energetic ion tails form simultaneously on both the T and He3 distribution functions. In this case, the iteration procedure between the full-wave and Fokker-Planck calculations must be generalized to include two non-Maxwellian species. To simplify the problem, it is assumed that the density of the high energy ions is low enough that collisions between the two developing tails can be neglected in the Fokker-Planck solution. The wave solution, however, allows both tails to interact self-consistently, and both contribute to the absorbed power. In Fig. 2, this model is applied to minority He^3 heating in ITER where

the minority fraction is assumed to be 3%. A single toroidal mode corresponding to n = -27 is considered. Radial profiles for the power absorption show that the largest fraction of power is absorbed by the minority He^3 (53%) while the remaining power goes to electrons (40%) and tritium (7%). The supra-thermal tail on the He^3 distribution has an equivalent temperature of about 168 keV, whereas the tail on the tritium is less energetic and less dense. This reflects the difference in heating mechanisms as well as the higher density of tritium. The second harmonic tritium interaction requires finite temperature to occur, whereas the fundamental minority He^3 interaction does not. Thus, there is more energy available to pull out a tail in the case of He^3 where wave interaction is at the fundamental. Also, the higher tritium density produces more collisions with the low energy bulk distribution, making tail formation more difficult.

5. Full-wave calculations of Lower Hybrid Propagation

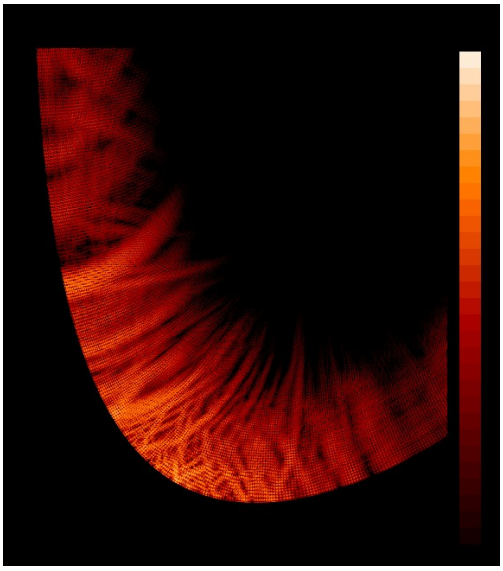

FIG. 3. Full wave lower hybrid simulation demonstrating resonance cone structures

In the lower hybrid frequency regime, defined by $\Omega_i \ll \omega \ll \Omega_e$, where $\Omega_{i,e}=qB/m_{i,e}c$ are the electron and ion cyclotron gyration frequencies in a magnetic field of strength B, plasma waves are nearly electrostatic and have very short wavelengths relative to equilibrium scale lengths. The waves are thus good candidates for a WKB approach such as ray tracing which has been the solution method of choice. However there are several known deficiencies with this approach. Lower hybrid waves are weakly damped and undergo multiple reflections from the low density cutoff at the edge of the plasma. The rays also propagate along characteristics of the electrostatic wave equation known as resonance cones (FIG. 3) that tend to become narrow and even singular at turning points forming caustics when they encircle the axis. Extended ray tracing techniques such as the Maslov method popular in seismology [18] and the wave-kinetic method [19], are valid at the caustic surfaces; but because the LH cutoffs in tokamak plasmas occur in the plasma edge where the gradients are very large and the wavelengths very long, they violate the WKB approximation where the plasma is changing on the same scale as the wavelength.

The full wave equation in Eqs.(1) may also be applied to the simulation of lower hybrid waves to overcome the above limitations of WKB theory. The TORIC code has been adapted [5] to that end. It solves the same wave equation as AORSA but in the basis,

$$\mathbf{E}(\mathbf{x}) = \sum_m \mathbf{E}_m(r) \exp\left(im\theta + in\phi\right)$$
$$k_{||} = (m\mathbf{B}\cdot\boldsymbol{\nabla}\theta + n\mathbf{B}\cdot\boldsymbol{\nabla}\phi)/B \quad , \qquad (3)$$

and with a dielectric appropriate for LHRF. The basis uses cubic finite elements for the flux direction and Fourier modes for the poloidal and toroidal directions. The dielectric in LHRF uses unmagnetized ion and zero finite Larmor radius electron responses and retains the fast (electromagnetic) and slow (electrostatic) branches of the dispersion while neglecting the

strongly evanescent ion plasma wave. TORICLH uses a non-Maxwellian distribution for electrons that can be specified or calculated by a Fokker-Planck code [20].

6. Comparisons with Ray Tracing

Calculations of propagation with the full wave approach show striking similarities and differences from the ray tracing approach. In FIG. 4 a typical ray is overlaid on a full wave result for a case with incomplete single pass absorption. The similarities between the ray trajectory and the field patterns are evident especially near the core. Power deposition demonstrates a strong disagreement between ray tracing and full wave. For the former, power is localized around a peak of $\sqrt{\psi_{tor}}$=0.4 and for the later a narrower peak about 0.8. For a given parallel wavenumber, $n_{||}$, the LH waves will damp according to the criterion, $n_{||} \approx 5.3/\sqrt{T_e[keV]}$ [21]. For the value of $n_{||}$=1.55 used in FIG. 4, single pass damping will occur at temperatures above 16 keV. At lower temperatures, reflections off cutoff near the wall play an important role. In reflectometry, it is known that these reflections cause scattering in the reflected spectrum and require a full wave treatment to accurately model [22]. As a consequence of this scattering as well as other diffractive processes, the waves phase velocity is down shifted sufficiently to damp at the lower temperatures in the outer plasma. The waves are accessible by the LH accessibility criteria [21] but are simply absorbed far from the core plasma. Analysis of the wavenumber spectrum of the solution confirms this is the case. The differences with ray tracing are reduced at higher temperatures in the single pass regime where core absorption is predicted by both codes. The radial locations still differ by about r/a~0.1 which can be attributed to focussing effects neglected in 1st order WKB damping theory. For the expected values of $n_{||}$=1.8—2.0 for an ITER LH antenna, ITER will be well into the single pass regime at 20 keV, which would imply that a 2nd order WKB model that retains the effects of focussing and spreading would have acceptable accuracy for predictive modelling.

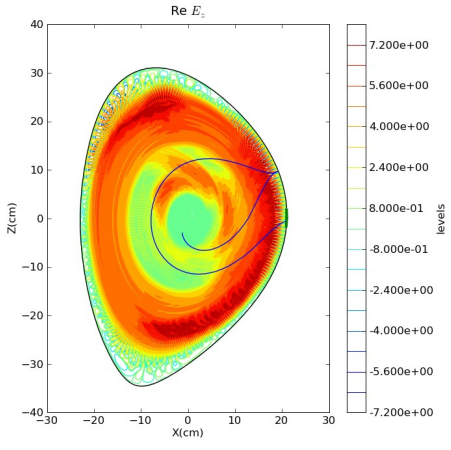

FIG. 4. Ray tracing path superimposed on a full wave result. Parameters are $n_{||}$=1.55, T_{e0}=12 keV, n_{e0}=4x10^{19}. *Resolution is 1080 radial elements by 2048 poloidal points.*

7. Non-Maxwellian Effects on Lower Hybrid Damping

The evolution of a quasilinear (QL) plateau is critical to take into account to have properly damping of the LH waves. TORIC can use a non-Maxwellian distribution specified either with an analytically defined QL plateau or generated by a CQL3D distribution. We find that the spectral broadening in the full wave LH simulations plays a dominant role in determining the location of power and current drive even in the presence of a QL effects. In FIG. 5 two full wave simulations using the non-Maxwellian distribution from a self-consistent ray tracing simulation using CQL3D/GENRAY are shown. The left figure limits the poloidal resolution to 256 mesh points which in turn limits how much spectral broadening can occur from scattering reflections from the wall. The power deposition for this case is very similar to that

seen in ray tracing. When the poloidal resolution is no longer limited, the scattering from reflections is resolved and large spectral broadening produces sufficiently slow phase velocities to damp in the cooler 1 keV plasma at a narrow layer around r/a~0.8.

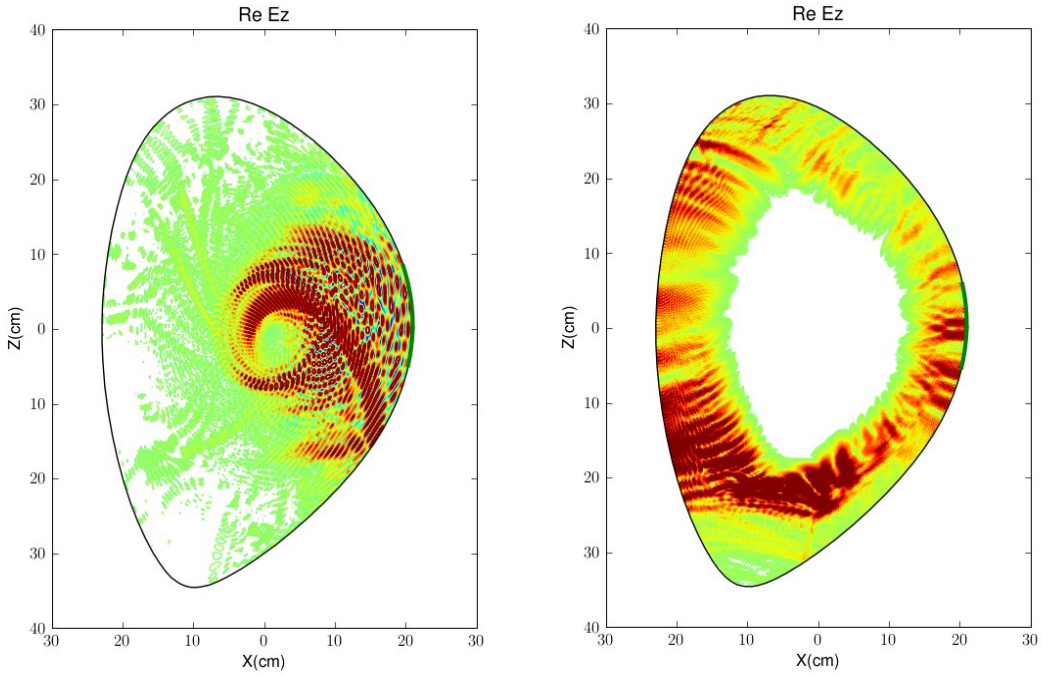

FIG. 5: Two full wave LH simulations use the same EQDSK Alcator C-Mod equilibrium and non-Maxwellian distribution from a CQL3D-GENRAY simulation. n_{e0} *=7×10¹³/cc,* T_{e0} *=2.3 keV,* B_0 *=5.4 T,* $n_{||}$=1.55. *Left figure, 256 poloidal elements, right figure 2048.*

8. Summary

In this paper, we have taken the first steps toward self-consistent 3D simulations of high power electromagnetic wave heating in the ITER burning plasma. ITER shows relatively strong focusing of the launched waves, while heating is localized in front of the antenna and near the plasma center. For minority He^3 heating scenarios, the ICRF interactions create energetic ion populations that can significantly affect the wave propagation and absorption and form simultaneously on both the T and He^3 distributions, although the tritium tail is less energetic and dense than that on the minority He^3. This is due in part to differences between fundamental and second harmonic ICRF interactions.

We have shown calculations of LH waves in toroidal geometry in a laboratory scale device. Realistic general geometry and non-Maxwellian electrons were used. These simulations predict quite different absorption locations for the waves than traditional ray tracing approaches in some regimes. In particular, it is seen that in multipass regimes, effects of reflections causes divergence between ray tracing and full wave predictions. The differences should be large enough to be validated experimentally.

References

[1] Aymar, R., Chuyanov, V. A., Huguet, M., Shimomura, Y., ITER Joint Central Team and ITER Home Teams, "The future international burning plasma experiment", Nucl. Fusion **41**, (2001) 1301.

[2] Start, D. F. H., Jacquinot, J., Bergeaud, V., et al., "D-T Fusion with Ion Cyclotron Resonance Heating in the JET Tokamak", Phys. Rev. Lett. **80**, (1998) 4681.

[3] Gormezano, C., Sips, A., Luce, T., et al., "Chapter 6: Plasma auxiliary heating and current drive", Nucl. Fusion, **47**, (2007), 2495.

[4] Pereverzev, G.V., "Use of the Multidimensional WKB Method to Describe Propagation of Lower Hybrid Waves in Tokamak Plasma", Nucl. Fusion **32**, (1992) 1091.

[5] Wright, J.C., Valeo, E.J., Phillips, C.K., Bonoli, P.T. and Brambilla, M., Commun. Comput. Phys., **4**, (2008), 545.

[6] Bonoli, P. T., Batchelor, D. B., Berry, L. A., et al., "Evolution of nonthermal particle distributions in radio frequency heating of fusion plasmas", J. Phys.: Conf. Ser., **78**, (2007), 012006.

[7] Jaeger, E.F., Berry, L.A., D'Azevedo, E., Batchelor, D. B. and Carter, M. D., need title, Phys. Plasmas. **8**, (2001), 1573.

[8] Brambilla, M., "Numerical simulation of ion cyclotron waves in tokamak plasmas", Plasma Phys. Control. Fusion **41**, (1999), 1.

[9] Wright, J.C., Bonoli, P.T., Brambilla, M., et al., "Full wave simulations of fast wave mode conversion and lower hybrid wave propagation in tokamaks", Phys. Plasmas **11**, (2004), 2473.

[10] Jaeger, E.F., Harvey, R., Berry, L., et al., Nucl. Fusion, **46**, (2006), S397.

[11] Jaeger, E.F., Berry, L.A., D'Azevedo, et al., Phys. Plasmas, **15**, (2008), 072513.

[12] Valeo, E.J., Phillips, C.K., Bonoli, P.T., and Wright, J.C., "Full-wave simulations of lh wave propagation in toroidal plasma with non-maxwellian electron distributions", in 17th Topical Conference on Radio Frequency Power in Plasmas, edited by Ryan, P. and Rasmussen, D., **933**, New York, (American Institute of Physics. 2007), 297.

[13] Bertelli, N., Pereverzev, G.V., and Poli, E., "Beam tracing description of lh waves in tokamaks", in 34th EPS Plasma Physics Conference, (2007).

[14] Stix, T.H., The Theory of Plasma Waves, 1992.

[15] Kennel, C.F. and Englemann, F., Phys. Fluids, **9** (1966) 2377.

[16] Harvey, R. W. and Mccoy, M. G., "The CQL3D Fokker-Planck Code ", IAEA (Montreal 1992), Proc. of the IAEA Tech. Committee Meeting, available through USDOC, NTIS No. DE9300962, Vienna (1993) 489-526.

[17] ITER Technical Basis Document (IAEA, Vienna, 2001) Doc. No. GAO FDR 1 00-07-13 R1.0, Section 4.3.3.

[18] Chapman, C.H. and Keer, H., "Application of the Maslov Seismogram Method in Three Dimensions", Stud. Geophys. Geo., **46** (2004) 615.

[19] Kupfer, K., Moreau, D., and Litaudon, X., "Statistical theory of wave propagation and multipass absorption for current drive in tokamaks", Phys. Fluids B, **5** (1993) 4391.

[20] Valeo, E. J. et al., "Full-wave simulations of lower hybrid wave propagation in toroidal plasma with nonthermal electron distributions, " 35th EPS Conference on Contr. Fusion and Plasma Phys., (2008).

[21] Bonoli, P., IEEE Trans. Plasma Sci., **PS-12**, (1984), 95-107.

[22] Lin, Y., Nazikian R., Irby, J. H. and Marmar, E. S., "Plasma curvature effects on microwave reflectometry fluctuation measurement ",Plasma Phys. Controlled Fusion, **43**, (2001), L1-L8.